Failure mapping of adhesively bonded single lap joints: nondimensional analysis

J.H. Tang, I. Sridhar*, N. Srikanth

School of Mechanical and Aerospace Engineering,
Nanyang Technological University, 50 Nanyang Avenue, Singapore 639798

Abstract

The debonding problem of single lap joints subjected to in-plane loading is analyzed based on nondimensional approach pioneered by Lai and co-authors [1]. This approach allows the determination of specific nondimensional energy release rate and prediction of debonding or adherend kinking mapping region. For equal moduli of adherend, the analysis reveals that asymmetrical configuration induces unfavorable conditions of higher debonding and kinking propensity. Compared to the experimental measurements, the analysis presented shows a fairly good agreement of expected failure mode for a given set of geometry and material parameters. The mapping of failure region from the nondimensional analysis is instructive as a design failure map for predicting the fracture behavior of asymmetrical single lap joints.

Keywords: single lap joint, debonding, crack kinking, mixed mode, tensile loading.

*Corresponding author.
Email address: msridhar@ntu.edu.sg (I. Sridhar)

Nomenclature

A_{e}, I_{e} geometric factors

A_i, B_i six out of eight unknowns of the linear algebraic equations where $i = 0, 1, 2$

D_i flexural rigidities of $i = 0, 1, 2$

E_1 Young's modulus of upper adherend

E_2 Young's modulus of lower adherend

$G_{0\mathrm{C}}$ fracture toughness of interfacial debonding

G_0 energy release rate of interfacial debonding

$G_{1\mathrm{C}}$ fracture toughness of kinking in upper adherend

G_1 energy release rate of kinking in upper adherend

L length of asymetrical single lap joint

L_B nondimensional overlap length

M bending moment

P axial load

P_{C} ultimate load

P_{R} reference load

P_i initiation load

R shear force

$\hat{G}_s$ specific nondimensional energy release rate

f, f_1 functional representations of $\hat{G}_s$

h_1 upper adherend thickness

h_2 lower adherend thickness

l_A upper adherend arm length

l_B overlap section length

l_C lower adherend arm length

q nondimensional left-hand crack tip position

r nondimensional right-hand crack tip position

x_i, w_i local coordinate system of upper adherend ($i = 0$), overlap joint section ($i = 1$), and lower adherend ($i = 2$)

$\hat{G}$ nondimensional energy release rate

$\hat{M}$ nondimensional bending moment

$\hat{P}$ nondimensional axial load

$\hat{R}$ nondimensional reaction force

Δ a nondimensional quantity in term of η and Σ

Σ modulus ratio of the upper adherend to lower adherend

α_n small angle between x_1 axis and P axis

η thickness ratio of the upper adherend to lower adherend

κ adherend thickness ratio

λ_i constant coefficients for the differential equations where $i = 0, 1, 2$

ν_1 Poisson ratio of upper adherend

ν_2 Poisson ratio of lower adherend

ψ phase angle or mode mixity

ψ_C critical phase angle

1. Introduction

Single lap joints have been widely studied as a joining configuration for adhesively bonded joints. Its simplicity in adherend preparation renders its prevalence in adhesively bonded design for structural applications. The use of polymer matrix composites in aerospace and automotive industries has driven the use of

adhesively bonded technique over conventional mechanical joining methods such as bolted and riveted connection, in consideration of reduction in stress concentration and occurrences of manufacturing defects triggered by the fastener holes.

The debonding problem of single lap joint has been traditionally approached by assessment of peel and shear stresses at the adhesive bondline. This so-called stress-based approach has its root in early classical analyses carried out by Volkersen as well as Goland and Reissner [2], and further modified and refined by various authors. A summary of analytical stress models by various authors available in literature is presented by da Silva et al [3]. The same debonding problem at the bondline has also been approached by means of linear-elastic fracture mechanics [4–7]. Predicting failure using this energy-based approach has its assumption in that macroscopic crack exists such that the single lap joint is inherently cracked and its fracture load is independent of whether such macrocrack exist or not in reality [5].

The design of single lap joint has multitude issues, especially when provision regarding adhesive and adherend material systems, and geometrical constraints are not clearly defined from beginning. In this regard, classical stress based approach becomes complicated as the prior knowledge of absolute material elastic properties are so crucial in calculating stress distribution along the bondline overlap length. This limitation could be overcome by formulating the debonding problem in nondimensional variables, which can be conveniently done using fracture mechanics approach. Lai et al [1] presented a nondimensional analysis of the debonding of lap shear joint. Following this analysis, several recommendations were given in view of designing a specimen with ideal geometry attributes that allow the stable evolution of debonding as well as improve the fracture effi-

ciency. Kafkalidis and Thouless [8] presented similar nondimensional form which attempts to included the effect of the adherend plastic deformation into the analysis, in which it was illustrated with cohesive zone modeling. The nondimensional form of interfacial toughness and yielding strength are shown be relevant parameters for the joint strength.

This paper attempts to revisit the nondimensional approach in the context of debonding of asymmetrical single lap joint, and further explores the possibility of quantifying the fracture behavior of lap joint in a more holistic manner. The motivation is to express the problem merely in terms of nondimensional parameters so that its representation can be implemented in perspective of joint design and material selection, where uncertainties are compounded when the problem of geometrical constraint, material system and adhesive system selections are simultaneously present. An attempt to combine the benefits of insight into failure behavior and managing flexibility of all essential joint parameters is given by introduction of a term called specific nondimensional energy release rate. Alternative design perspective could be offered as integration of both designing and mechanics aspects in joint analysis is emphasized. The solution of the nondimensional representation is illustrated by mapping it onto failure region defined by load and geometrical parameters. The crack kinking from the interface to adherend of brittle adherend is also explored.

2. Problem description

2.1. Transverse deflection

The nondimensionalized approach developed by Lai et al [1] is adopted in current study, with special regard to debonding behavior of single lap joint. A

macroscopic cracked single lap joint specimen configuration and related parameters are shown in Figure 1. Modifications are made to accommodate for possibility of asymmetrical single lap joint configuration. When a crack is initiated, it usually starts at the location of high stress concentration. Two possible critical locations of potential crack initiation and their locations of crack tip, i.e. left-hand crack tip and right-hand crack tip are shown in Figure 1(a), and the bonded/uncracked overlap region is darkened for clarity. Adhesive layer is assumed to be very thin compared to adherend so that its thickness can be neglected.

Three sets of local coordinate systems (x_1, w_1), (x_0, w_0) and (x_2, w_2) are assigned, as illustrated in Figure 1(b), where w_1, w_0 and w_2 represent the transverse deflection of the specimen's neutral plane at x_1, x_0 and x_2 respectively. The force equilibrium and sign convention of the bending moment M, reaction/shear force R and axial force P are shown in Figure 1(c). The differential equations for transverse deflection, w_1, w_0 and w_2 are given by:

$$\frac{\mathrm{d}^2 w_1}{\mathrm{d}x_1^2} = -\frac{M_1}{D_1} = -\frac{P}{D_1}\left(\alpha_n x_1 - w_1 + \frac{R_A}{P}x_1 + \frac{M_A}{P}\right) \tag{1}$$

$$\begin{aligned}\frac{\mathrm{d}^2 w_0}{\mathrm{d}x_0^2} &= -\frac{M_0}{D_0} = -\frac{P}{D_0}\Bigg(\alpha_n\left(x_0 + l_A\right) \\ &\quad -w_0 - \left(\frac{h_1}{2} + h_2 - \Delta h_1\right) + \frac{R_A}{P}\left(x_0 + l_A\right) + \frac{M_A}{P}\Bigg)\end{aligned} \tag{2}$$

$$\begin{aligned}\frac{\mathrm{d}^2 w_2}{\mathrm{d}x_2^2} &= -\frac{M_2}{D_2} = -\frac{P}{D_2}\Bigg(\alpha_n\left(x_2 + l_A + l_B\right) \\ &\quad -w_2 - \frac{1}{2}\left(h_1 + h_2\right) + \frac{R_A}{P}\left(x_2 + l_A + l_B\right) + \frac{M_A}{P}\Bigg)\end{aligned} \tag{3}$$

where D_1, D_0 and D_2 are the flexural rigidities of the upper adherend, overlap joint section, and lower adherend, respectively, whereas the following notations are made consistent with those given by Lai et al [1]:

Δ is a nondimensional quantity: $\Delta = \dfrac{1+2\Sigma\eta+\Sigma\eta^2}{2\eta\,(1+\Sigma\eta)}$,

η is the thickness ratio of the upper adherend to lower adherend: $\eta = h_1/h_2$,

Σ is the modulus ratio of the upper adherend to lower adherend: $\Sigma = E_1^*/E_2^*$,

$E_1^* = E_1/(1-\nu_1^2)$ and $E_2^* = E_2/(1-\nu_2^2)$ for the plane strain cases,

$E_1^* = E_1$ and $E_2^* = E_2$ for the plane stress cases,

and α_n represents the angle between the x_1 (or x_2) horizontal axis and the axis of applied load:

$$\alpha_n = \frac{1}{2}\,(h_1+h_2)\,/L$$

The solutions of equations (1) to (3) are given by:

$$\begin{aligned}\frac{w_1}{L} &= A_1\cosh(\lambda_1 x_1)+B_1\sinh(\lambda_1 x_1)\\ &\quad +(\alpha_n+\hat{R}_A)\frac{x_1}{L}+\hat{M}_A \qquad (4)\end{aligned}$$

$$\begin{aligned}\frac{w_0}{L} &= A_0\cosh(\lambda_0 x_0)+B_0\sinh(\lambda_0 x_0)\\ &\quad +(\alpha_n+\hat{R}_A)\frac{(x_0+l_A)}{L}-\frac{1}{L}\left(\frac{h_1}{2}+h_2-\Delta h_1\right)+\hat{M}_A \qquad (5)\end{aligned}$$

$$\begin{aligned}\frac{w_2}{L} &= A_2\cosh(\lambda_2 x_2)+B_2\sinh(\lambda_2 x_2)\\ &\quad +(\alpha_n+\hat{R}_A)\frac{(x_2+l_A+l_B)}{L}-\alpha_n+\hat{M}_A \qquad (6)\end{aligned}$$

respectively, where

$$\lambda_1 = \sqrt{\frac{P}{D_1}}, \quad \lambda_0 = \sqrt{\frac{P}{D_0}}, \quad \lambda_2 = \sqrt{\frac{P}{D_2}}$$

and $\hat{R_A}$ and $\hat{M_A}$ are the nondimensional reaction force and reaction moment which are given by

$$\hat{R}_A = \frac{R_A}{P} \qquad \text{and} \qquad \hat{M}_A = \frac{M_A}{PL}$$

respectively. The eight unknowns, A_1, B_1, A_0, B_0, A_2, B_2, $\hat{R}_A$ and $\hat{M}_A$ in equations (4) to (6) can be solved by imposing appropriate eight boundary conditions. A set of linear algebraic equations as a result of these boundary conditions may be simplified by additional notations provided in AppendixA.

2.2. Energy release rate and mode mixity

The nondimensional energy release rate for the left-hand crack tip to propagate (which in effect also similar to one derived by Lai et al [1] for a cracked lap shear joint) can be written as:

$$\begin{aligned}
\hat{G} &= G/\frac{P^2}{(E_1^* + E_2^*)(h_1 + h_2)} \\
&= \frac{1}{2}\left\{ \left(1+\frac{1}{\Sigma}\right)\left[\left(1+\frac{1}{\eta}\right) + 12\hat{M}_1^2\left(1+\frac{1}{\eta}\right)^3\right] \right. \\
&\qquad \left. -(1+\Sigma)\left[\frac{(1+1/\eta)}{A_e} + \hat{M}_0^2\frac{(1+1/\eta)^3}{I_e}\right]\right\} \qquad (7)
\end{aligned}$$

where $\hat{M}_1$ and $\hat{M}_0$ are the nondimensional bending moments given by

$$\hat{M}_1 = \frac{M_1(l_A)}{P(h_1+h_2)} \qquad \text{and} \qquad \hat{M}_0 = \frac{M_0(0)}{P(h_1+h_2)}$$

whereby both bending moments are respectively evaluated at $x_1 = l_A^-$ and $x_0 = 0^+$. Using the additional notations introduced in Appendix A, it can be readily shown that the nondimensional energy release rate can be implicitly and fully described by the six nondimensional (load, geometrical and material) parameters. Specifically, the debonding problem of the asymmetrical single lap joint could be described in terms of these six parameters: nondimensional axial load, $\hat{P} = \sqrt{P/E_1^*(h_1+h_2)}$; nondimensional left-hand crack tip position, $q = l_A/L$; nondimensional right-hand crack tip position, $r = l_C/L$; nondimensional first or upper adherend thickness, $\kappa = h_1/L$; adherend thickness ratio, $\eta = h_1/h_2$ and adherend modulus ratio, $\Sigma = E_1^*/E_2^*$, which are again made to be consistent with those given by Lai et al [1]. The geometric factors A_e and I_e, as well as expression for evaluation of global mode mixity are defined and given in AppendixB1.

The effect of boundary conditions on the energy release rate and global mode mixity are reflected through the expressions of nondimensional bending moments, $\hat{M}_1$ and $\hat{M}_0$, in addition to the axial load P. In essence, the energy release rate is not merely explicitly expressed as a quadratic function of P but also through some implicit nonlinear function of P. Further, it is essential to look into the energy release rate for the competing debonding side: right-hand crack tip of the single lap joint. Its nondimensional energy release rate and mode mixity are separately given in AppendixB.2. The effect of micro crack initiated by dislocation piled up on the energy release rate and mode mixity is not considered in this study. This type of analysis is found elsewhere [9–11].

2.3. *Nondimensional representation of solution*

Using functional representation, equation (7) can be generalized as

$$\hat{G}_s = f\left(\Sigma, \eta, q, r, \kappa, P/P_{\mathrm{R}}\right) \tag{8}$$

where $\hat{G}_s$ may be henceforth called the *specific nondimensional energy release rate* which is given by $G(E_1^* + E_2^*)/[E_1^{*2}(h_1 + h_2)]$. Reference load P_{R} is expressed as $E_1^*(h_1 + h_2)$. P/P_{R} may be called the specific loading ratio, and its practical value is usually less than 10^{-2}.

If any four parameters of $\hat{G}_s$ could be constrainted, the remaining two parameters could be mapped into a 2-dimensional failure region whereby it might serve as a design map for better understanding the debonding problem of an asymmetrical single lap joint. Particularly from design perspective, it is deemed useful to have the effect of P/P_{R} or overlap length ratio $L_B = l_B/L = (1 - q - r)$ on the $\hat{G}_s$ being investigated. Thus, it may be more convenient to contraint $q = r$, and have the angle α_n fixed such that geometrical scaling of the problem could be collectively examined. With such reinterpretation, equation (8) reduced to

$$\hat{G}_s = f_1\left(\Sigma, \eta, L_B, \alpha_n, P/P_{\mathrm{R}}\right) \tag{9}$$

2.4. *Kinking consideration*

The results presented by He and Hutchinson [12] suggest that the ratio of energy release rate of kinking in material 1 (herein restrict the discussion to left-hand crack) to that interfacial debonding, i.e. G_1/G_0, depends on phase angle or mode mixity ψ of interface crack, and the modulus ratio Σ. In the current

analysis, the effect of in-plane (T) stress described by He et al [13] is nullified by zeroing the length of the kinked crack for simplicity. It is recognized that the non-uniform in-plane stress caused by the axial load does influence the kinking behavior, and because the in-plane stress tends to increase the kinking energy release rate, any kinking condition fufilled herein may be interpreted as definite occurence of kinking.

A special result whereby $\Sigma = 1$ is demonstrated here. The approximate values G_1/G_0 for different ψ are given in Figure 2. It is implied that G_1/G_0 is amount of maximum energy release rate attainable in kinking direction, and this attainable energy release rate depends on magnitude of phase angle. The kinking direction (kinked angle) is not unique as it varies with phase angle [12], and therefore not emphasized and further elaborated in current study. Hence, Figure 2 should be interpreted with such awareness in mind: presuming kinking occurs in material 1, there will be a unique (absolute value of) phase angle where the energy release rate is found to be maximum. The actual sign of phase angle when kinking occurs depends on whether that material is modeled at the top (hence negative sign) or bottom (positive sign) of the interface. Should material 2 is modeled at the top, replace G_1 with G_2, and G_{1C} with G_{2C} in Figure 2. Note that, for $0 < \psi < 63^\circ$, the higher the ψ is, the higher the propensity of crack kinking into adherend layer.

Alternatively, Figure 2 could be adopted to judge whether failure mode is kinking or debonding dominant, simply determine the critical phase angle ψ_C from ratio of fracture toughness of material 1 to interfacial G_{1C}/G_{0C}. For a given bi-material system, a unique G_{1C}/G_{0C} value is predefined, the kinking condition is fulfilled whenever $G_{1C}/G_{0C} < G_1/G_0$, and this inequality is only fulfilled when

ψ is equal to or greater than ψ_C. When ψ is less than ψ_C, G_1/G_0 will always be less than G_{1C}/G_{0C}, so that kinking condition would inherently not be satisfied. For example, if given that $G_{1C}/G_{0C} \simeq 1.75$ (and hence $\psi_C \simeq 55^\circ$), any $\psi > \psi_C$ is kinking dominant, whereas any $0 < \psi < \psi_C$ is debonding dominant. At $\psi \simeq 63^\circ$, G_1/G_0 becomes maximum at approximate value of 1.8, which suggests that once G_{1C}/G_{0C} is greater than 1.8, kinking is totally inhibited, leaving debonding as the only possible failure mode, regardless of ψ value.

3. Experimental verification

To demonstrate the practicality of the nondimensional approach, a series of tensile tests were conducted using the single lap joint specimens with which adherends were made of polymethyl methacrylate (PMMA), tradename Plexiglas, and adhesively bonded using Araldite 90 minutes epoxy or Acrifix 192 methylmethacrylate adhesives. Both symmetrical and asymmetrical configurations were being investigated. The dimensions of specimens are given in Table 1. Five specimens were tested for each configuration. Note that how certain specimen configurations belonged to identical nondimensional parameter groups. Also, realize that special case $\Sigma = 1$ and $\alpha_n = 0.025$ are being investigated here.

Araldite 90 minutes was used to simulate the debonding failure, due to its weak adhesion with PMMA. Contrary, Acrifix 192 was used to promote the possibility of kinking failure of adherends, due to its strong adhesion with PMMA. The adhesive thickness was controlled using fiber mesh of 0.23 mm thick. The mode I and mode II fracture energies of Araldite adhesive system are 12.2 J/m^2 and 84.0 J/m^2, respectively, determined using double cantilever beam and end notched flexure tests. The fracture energy of Acrifix adhesive system are assumed

to be at least as great as the fracture toughness of PMMA, which was found to be 756 J/m^2, determined from single edge notched beam specimens. This assumption is justified since Acrifix 192 is a reaction adhesive based on MMA polymerization, whereby partial dissolution of the PMMA adherend surface by the monomer causes the polymer chain to swell and become entangled. Additionally, an explicit measurement of fracture toughness for the Acrifix system does not give any meaningful interpretation since the joint failure for Acrifix adhesive system occurs exclusively at the adherend. It is noted that a lower fracture toughness value was evaluated using single edge notched specimens with longer crack length (0.1 mm versus 0.04 mm), but only the higher toughness value was reported here as a shorter crack length echoes the occurrence of a kinked crack from the glossy surface of PMMA adherend.

Prior to bonding, the adherends were annealed at 80 °C for 3 hours in oven, to avoid any stress cracking. An initial debonding of about 0.5 mm length was purposely created, by means of masking of non-porous teflon sheet, in all specimens in order to trigger a macroscopic crack. The specimens were loaded to its ultimate failure using Instron 5569 Universal Testing Machine at a crosshead displacement controlled at a rate of 0.5 mm/min, where clamped-clamped condition prevails at both loading ends. Because of the transparency of PMMA, the interfacial initiation of the specimens made of Araldite adhesive system was convenient to be visually identified and its initiation load could thus be measured. Meanwhile, kinking of the specimens made of Acrifix adhesive system only led to catastrophic failure, thereby requiring no distinction be given between its initiation and catastrophic end failure load, compared to Araldite adhesive system.

4. Results and discussions

4.1. Theoretical interpretation

Theoretical interpretation of equation (9) is demonstrated by means of a specific solution upon imposing $\Sigma = 1$ and $\alpha_n = 0.025$ with clamped-clamped boundary condition. As per experimental design: $\alpha_n = 0.025$ relatively indicates a rather high value of total adherends thickness is being selected for investigation, for no specific reason.

The fracture behavior of changing the thickness ratio η of single lap joint, in particular inducing an asymmetrical configuration, can be best depicted using Figures 3 and 4. Cases whereby $\eta = 1$ and $\eta = 0.33$ have been chosen for comparison. In term of likelihood for debonding from the left-hand crack tip, it can be noted that asymmetrical configuration induces a higher $\hat{G}_s$ for the same loading ratio P/P_{R}, as illustrated by comparing contour lines between Figures 3(a) and 4(a). Pertaining to whether a debonding from right-hand crack tip is favored, it can be shown, using analysis presented in Appendix B, that the $\hat{G}_s$ is always lower than that from the left-hand crack tip, such that this possibility is rejected.

The phase angle ψ is uniquely important for predicting the kinking problem, that is adherend brittle failure, in single lap joint. The phase angle contours correspond to $\hat{G}_s$ in Figures 3(a) and 4(a) are illustrated by Figures 3(b) and 4(b), respectively. A negative phase angle suggests that the upper adherend is the one which subjected to kinking. Boundary separating the region of kinking or debonding may be determined by considering ψ_{C}. For example, if given that $G_{1\mathrm{C}}/G_{0\mathrm{C}} \simeq 1.75$ (and hence $\psi_{\mathrm{C}} \simeq 55^{\circ}$), any region $|\psi| > \psi_{\mathrm{C}}$, as appears in Figure 3(b), is tend to be kinking dominant. Likewise, any region $0 < |\psi| < \psi_{\mathrm{C}}$

is tend to be debonding dominant. Therefore, comparison between $|\psi|$ in Figures 3(b) and 4(b) infers that kinking tends to be favorable in asymmetrical configuration. The required $\hat{G}_s$ for kinking problem could be obtained by multiplying $\hat{G}_s$ for debonding problem with G_1/G_0 which in turn depends on $|\psi|$. As shown in Figure 2, this G_1/G_0 should vary between value of 1 to 1.8.

From analysis presented herein, interpretations derived from Figure 3 or 4 could be conceived as mapping the design region for understanding the debonding, as well as the kinking behavior, of asymmetrical single lap joint.

4.2. Experimental validation

The failure mode for Araldite adhesive system is interfacial [see Figure 5(a)] for all the specimens tested, thus simulating the debonding problem of the single lap joint. The failure initiation load was found to be much lower than the ultimate load, as listed in Table 2, especially for joint with high overlap length. Here, the critical values $\hat{G}_s$ were calculated by taking only mode I fracture toughness into account. The failure points, thus based on data given in Table 2, for debonding failure of specimens, are summarized in Figure 6. The circular and square makers represent the experimentally determined $\hat{G}_s$ while the solid contour lines with values of 1.1 and 1.7 represent the predicted $\hat{G}_s$, respectively, for total nominal thickness $h_1 + h_2$ of 4 mm and 6 mm at overlap region. Despite of two different geometrical configurations in term of total thickness, they could be nondimensionally described as identical problem.

It could be noted that fluctuations in Araldite system is rather big, probably because of big scatter in fracture toughness, as this was noticed from the double cantilever specimens. It is deemed inconsistency in the distribution of void for-

mation during mixing of Araldite resin has a part to play. This behavior is more evident in specimens with total nominal thickness of 6 mm. Comparison of effect of η can be made between Figures 6(a) and 6(b), in which it is shown that asymmetrical configuration indeed results in lower initiation load. Thus, asymmetrical single lap joint should be avoided unless it is necessary otherwise due to design constraint. In Figure 6(b), the experimentally determined $\hat{G}_s$ appears to be higher than predicted for $L_B > 0.3$, probably because mixed mode interaction becomes more important, as the the phase angle increases with higher overlap length, as seen from Figure 4(b).

Meanwhile, the failure mode for single lap joints with Acrifix adhesive system is solely brittle cracking of adherends, thus actually simulating the kinking problem of single lap joint [see Figure 5(b)]. For Acrifix adhesive system, $G_{1C}/G_{0C} \simeq 1.0$, and thus from Figure 2, any region of $|\psi| > 0$ is kinking dominant. The failure load data are given in Table 3, where failure is only catastrophic in nature. From Figure 3(b), the value of phase angle for $0.1 < L_B < 0.5$ is ranging from 50° to 60°. Because of kinking, the contour value of $\hat{G}_s$ is to be increased by a factor, $G_1/G_0 \simeq 1.75$, which can be estimated from Figure 2 for $\psi_C \simeq 55°$. After which, the failure points for the specimens with Acrifix system can be summarized in Figure 7. A good agreement between prediction and experiment is noted. Notice that due to adherend fracture mode, the determined $\hat{G}_s$ is almost two orders higher than that of joint with Araldite adhesive system.

A question may be raised pertaining to how the fracture behavior will be affected by the inclusion of adhesive layer. Albeit there are three materials involved in the analysis, it is not difficult to understand from a simple energy argument or application of J-integral, whether a crack remains within the adhesive layer

or interface, the same amount of strain energy is released as the crack advances. Complication arises when there is a shift in phase angle between the local (microscopic) and global (macroscopic) applied stress intensities, which in turn affects the interpretation of kinking propensity as well as change in critical fracture energy. In view of these complexities, the discussions in this paper only focus on giving an overview of how the nondimensional approach might be implemented in interfacial as well as kinking problem of adhesively bonded joint, from the global (macroscopic) point of view which neglects the finite adhesive layer thickness. A detailed discussion of crack trapping within the adhesive layer, along the interface, stability of crack trapping, and the selection of interface or in-layer cracking may be more appropriately found elsewhere [14–17].

5. Conclusions

This work conceives the nondimensional representation for the debonding problem of asymmetrical single lap joint. This nondimensional approach allows the consolidation of all load, geometrical and material parameters into single analysis, by presenting the solution into specific nondimensional energy release rate $\hat{G}_s$ and mode mixity ψ. For equal moduli of both adherends, the mapping of $\hat{G}_s$ shows that asymmetrical configuration induces higher $\hat{G}_s$, while that of ψ shows a propensity of kinking increases with asymmetrical design. For these reasons, asymmetrical single lap joint should be avoided. Because of nondimensional representation, the problem pertaining to scaling of geometrical configuration can be easily analyzed. Experimental validation shows reasonable accuracy was predicted by the nondimensional representation, concerning the fracture behavior of single lap joint. The nondimensional approach offers a new paradigm in design

process as material selection, adhesive system selection, geometrical scaling of the single lap joint could be combined into one step.

Acknowledgment

J.H. Tang appreciates the financial support from Nanyang Technological University in the form of graduate assistantship and I. Sridhar thanks Energy Research Institute at NTU (ERI@N) for additional financial support in bonded joints for turbine blades design.

References

[1] Lai YH, Rakestraw D, Dillard DA. The cracked lap shear specimen revisited-a closed form solution. Int J Solids Struct 1996;33:1725–43.

[2] Goland M, Reissner E. The stresses in cemented joints. J Appl Mech 1944; 11:A17–A27.

[3] da Silva LFM, das Neves PJC, Adams RD, Spelt JK. Analytical models of adhesively bonded joints-Part I. Literature survey. Int J Adhes Adhes 2009; 29:319–30.

[4] Anderson GP, Brinton DH, Ninow KJ, DeVries KL. Fracture mechanics approach to predicting bond strength. ASME, Mater Div (Publ) 1988;6:93–9.

[5] Fernlund G, Papini M, McCammond D, Spelt JK. Fracture load predictions for adhesive joints. Compos Sci Technol 1994;51:587–600.

[6] Shahin K, Taheri F. The strain energy release rates in adhesively bonded balanced and unbalanced specimens and lap joints. Int J Solids Struct 2008; 45:6284–300.

[7] Luo Q, Tong L. Fracture prediction of adhesively bonded structures using energy release rates. J Adhes Sci Technol 2009;23:1415–40.

[8] Kafkalidis MS, Thouless MD. The effects of geometry and material properties on the fracture of single lap-shear joints. Int J Solids Struct 2002; 39:4367–83.

[9] Cherpanov G. Interface microcrak nucletion. J Mech Phys Solids 1994; 42:665–80.

[10] Fan H, Xiao ZM. A zener-stroh crack near an interface. Int J Solids Struct 1997;34:2829–42.

[11] Chen BJ, Xiao ZM, Liew KM. Electro-elastic stress analysis for a wedge-shaped crack interacting with a screw dislocation in piezoelectric solid. Int J Eng Sci 2002;40:621–35.

[12] He MY, Hutchinson JW. Kinking of a crack out of an interface. J Appl Mech, Trans ASME 1989;56:270–8.

[13] He MY, Bartlett A, Evans AG, Hutchinson JW. Kinking of a crack out of an interface: role of in-plane stress. J Am Ceram Soc 1991;74:767–71.

[14] Wang SS, Mandell JF, McGarry FJ. An analysis of the crack tip stress field in dcb adhesive fracture specimens. Int J Fract 1978;14:39–58.

[15] Fleck NA, Hutchinson JW, Suo Z. Crack path selection in a brittle adhesive layer. Int J Solids Struct 1991;27:1683–703.

[16] Hutchinson JW, Suo Z. Mixed mode cracking in layered materials. Adv Appl Mech 1991;29:63–191.

[17] Akisanya AR, Fleck NA. Analysis of a wavy crack in sandwich specimens. Int J Fract 1992;55:29–45.

[18] Suo Z, Hutchinson JW. Interface crack between two elastic layers. Int J Fract 1990;43:1–18.

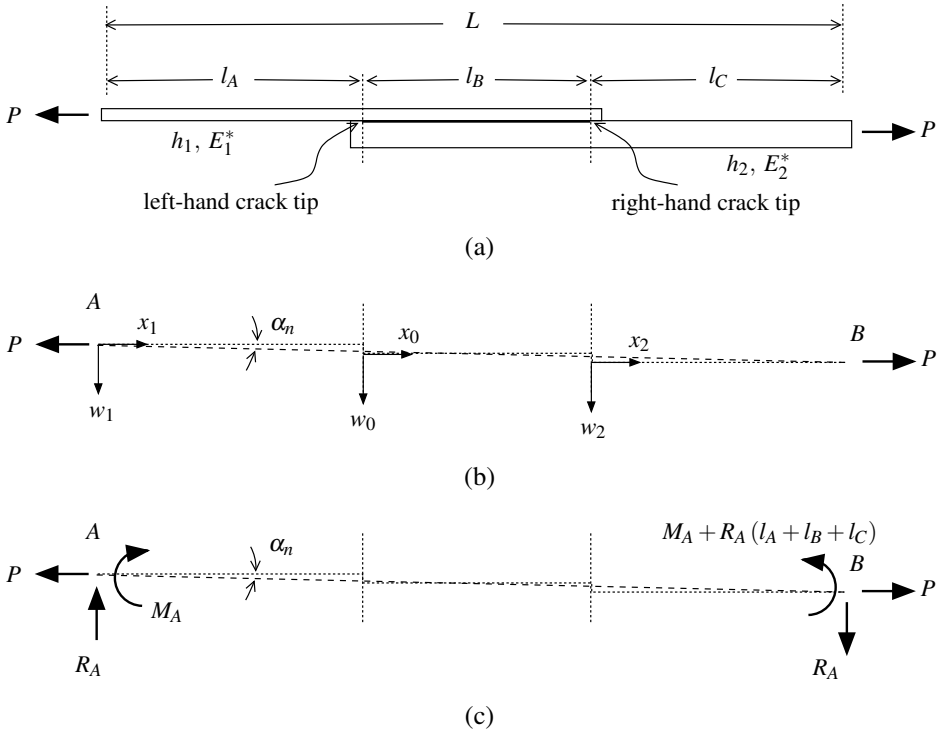

Figure 1: Schematic illustration of (a) geometrical configuration and material variables (b) all coordinate systems (c) external end forces of an asymmetrical single lap joint specimen.

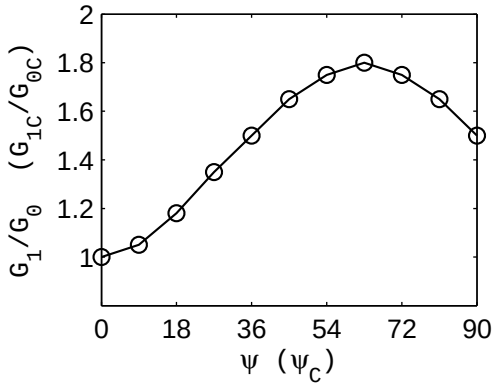

Figure 2: Approximate values of G_1/G_0 for different ψ [12].

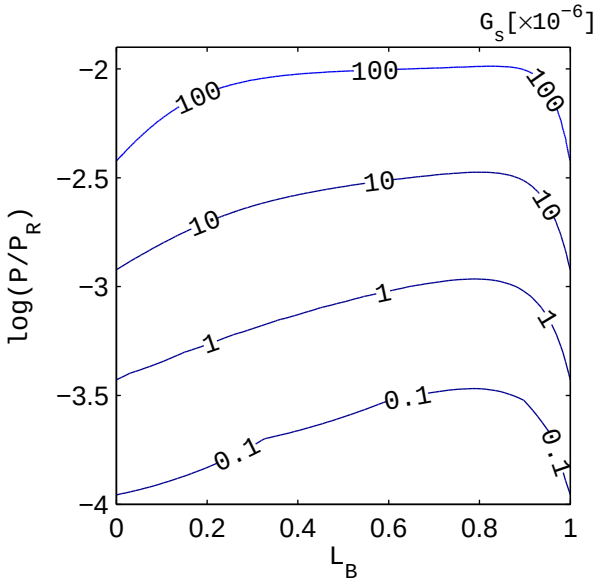

(a)

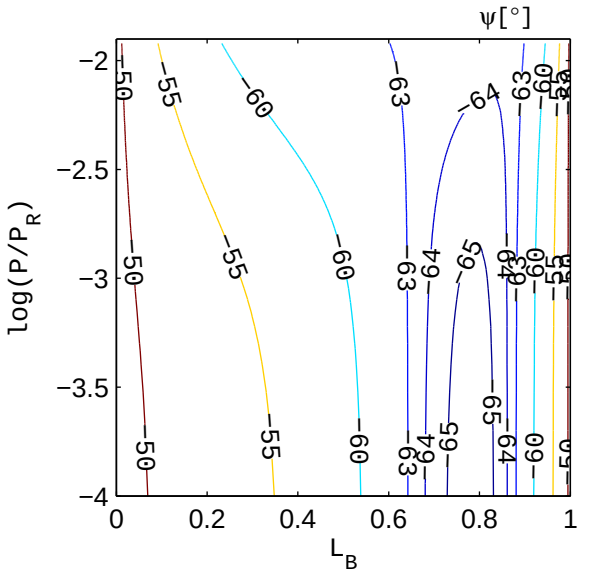

(b)

Figure 3: Contours of (a) specific nondimensional energy release rate $\hat{G}_s$ (b) phase angle ψ, for the case of $\eta = 1$ in load ratio and overlap length space.

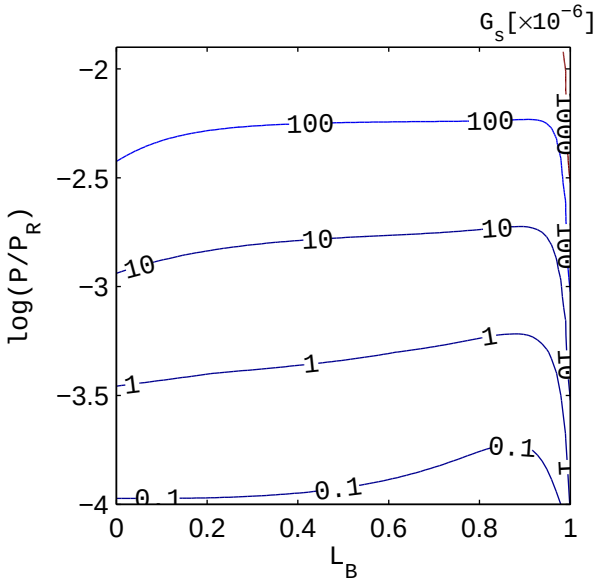

(a)

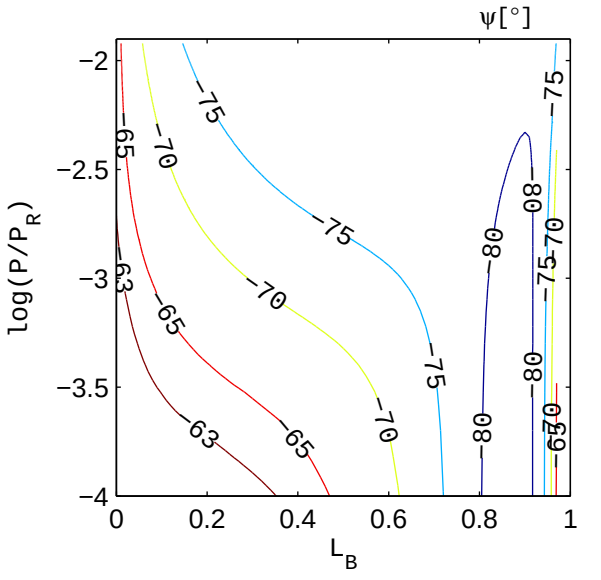

(b)

Figure 4: Contours of (a) specific nondimensional energy release rate $\hat{G}_s$ (b) phase angle ψ, for the case of $\eta = 0.33$ in load ratio and overlap length space.

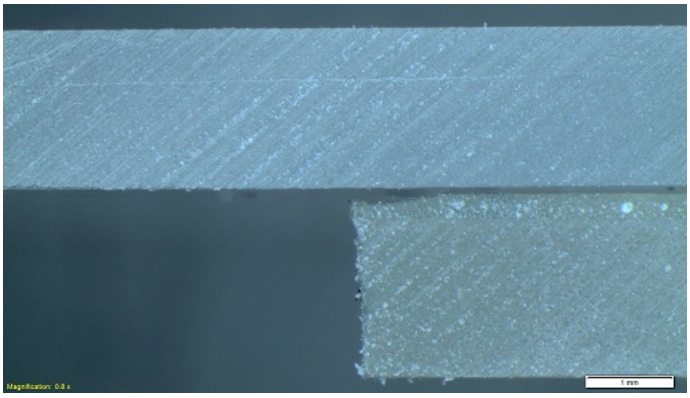

(a)

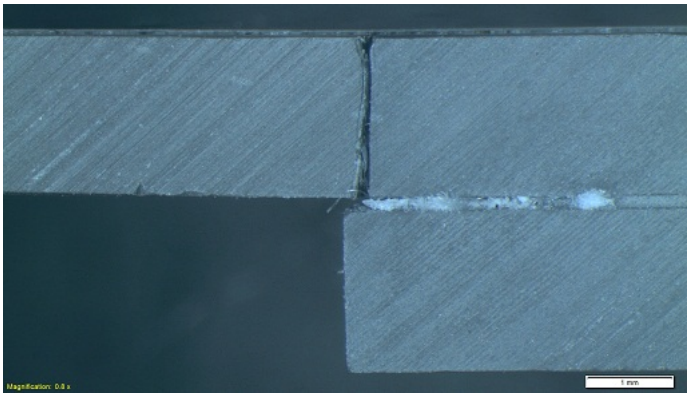

(b)

Figure 5: Photographs of (a) interfacial debonding (b) kinking failure of joint with nominal thickness $h_1 = h_2 = 2\,\text{mm}$.

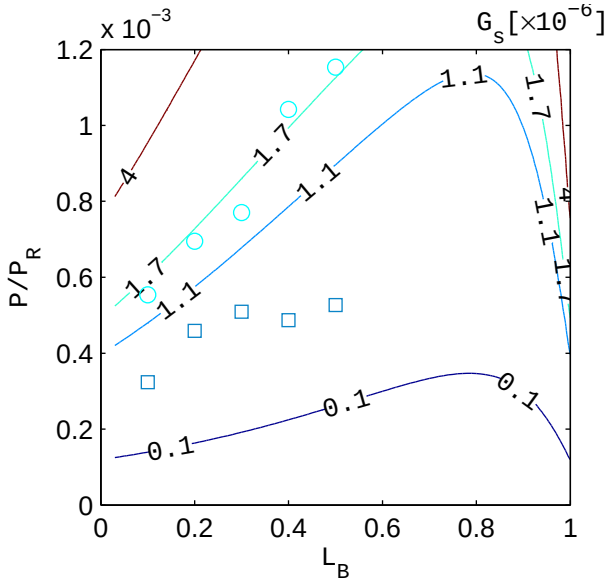

(a)

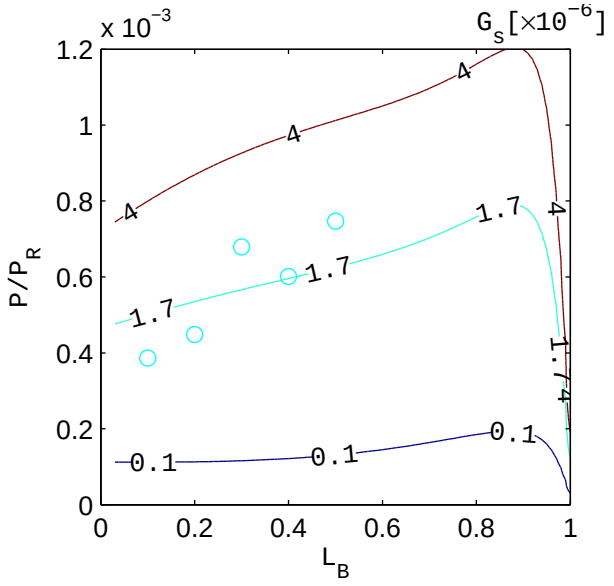

(b)

Figure 6: Comparison of $\hat{G}_s$ for the case of (a) $\eta = 1$ (b) $\eta = 0.33$, and joint's failure with adherend kinking mode. Circular marker: total nominal thickness = 4 mm; square marker: total nominal thickness = 6 mm.

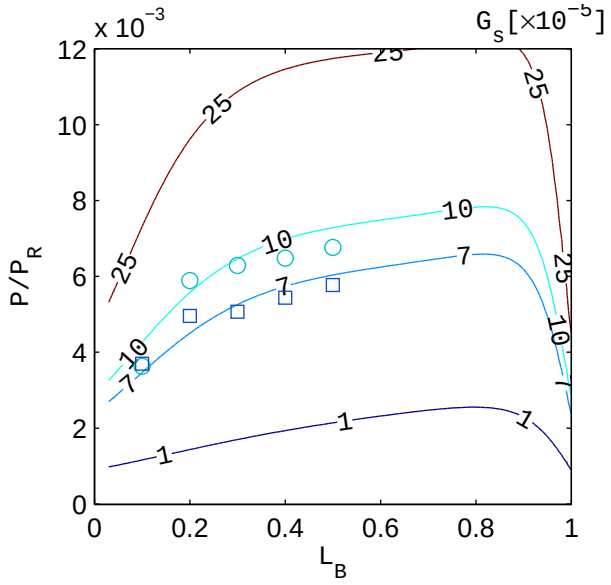

Figure 7: Comparison of $\hat{G}_s$ for the case of $\eta = 1$, and joint's failure with adherend kinking mode. Circular marker: total nominal thickness = 4 mm; square marker: total nominal thickness = 6 mm.

Table 1: Single lap joint specimens dimensions.

Adhesive system	h_1 [mm]	h_2 [mm]	η	L [mm]	l_B [mm]	L_B
Araldite or Acrifix	2	2	1.00	80	8	0.1
					16	0.2
					24	0.3
					32	0.4
					40	0.5
Araldite or Acrifix	3	3	1.00	120	12	0.1
					24	0.2
					36	0.3
					48	0.4
					60	0.5
Araldite only	1	3	0.33	80	8	0.1
					16	0.2
					24	0.3
					32	0.4
					40	0.5

Table 2: Test results for single lap joints with Araldite adhesive system.

L [mm]	l_B [mm]	L_B	G_{0C} [J/m^2]	$\hat{G}_s$ at G_{0C} [$\times 10^{-6}$]	Initiation load, P_i [kN/m]	Ultimate load, P_C [kN/m]	P_i/P_R [$\times 10^{-4}$]
$h_1 = 2$ mm, $h_2 = 2$ mm, total thickness at overlap region = 4 mm, $E_1 = E_2 = 3.3$ GPa, $\nu_1 = \nu_2 = 0.37$							
80	8	0.1	12.2	1.68	8.0	8.6	5.54
	16	0.2			10.1	11.0	6.95
	24	0.3			11.2	13.4	7.70
	32	0.4			15.1	16.5	10.42
	40	0.5			16.8	18.5	11.54
$h_1 = 3$ mm, $h_2 = 3$ mm, total thickness at overlap region = 6 mm, $E_1 = E_2 = 3.3$ GPa, $\nu_1 = \nu_2 = 0.37$							
120	12	0.1	12.2	1.12	7.0	9.0	3.23
	24	0.2			10.0	11.4	4.59
	36	0.3			11.1	14.2	5.09
	48	0.4			10.6	13.3	4.87
	60	0.5			11.5	19.9	5.27
$h_1 = 1$ mm, $h_2 = 3$ mm, total thickness at overlap region = 4 mm, $E_1 = E_2 = 3.3$ GPa, $\nu_1 = \nu_2 = 0.37$							
80	8	0.1	12.2	1.68	5.9	6.4	3.86
	16	0.2			6.9	9.0	4.48
	24	0.3			10.4	13.7	6.79
	32	0.4			9.2	13.0	6.00
	40	0.5			11.4	17.6	7.47

Table 3: Test results for single lap joints with Acrifix adhesive system.

L [mm]	l_B [mm]	L_B	G_{1C} [J/m^2]	$\hat{G}_s$ at G_{1C} [$\times 10^{-5}$]	Ultimate load, P_C [kN/m]	P_C/P_R [$\times 10^{-3}$]
$h_1 = 1.9$ mm, $h_2 = 1.9$ mm, total thickness at overlap region = 4.1 mm, $E_1 = E_2 = 3.3$ GPa, $\nu_1 = \nu_2 = 0.37$						
80	8	0.1	756	10.4	52.7	3.63
	16	0.2			85.6	5.89
	24	0.3			91.4	6.29
	32	0.4			94.1	6.48
	40	0.5			98.2	6.76
$h_1 = 2.8$ mm, $h_2 = 2.8$ mm, total thickness at overlap region = 5.8 mm, $E_1 = E_2 = 3.3$ GPa, $\nu_1 = \nu_2 = 0.37$						
120	12	0.1	756	7.06	79.1	3.70
	24	0.2			106.1	4.96
	36	0.3			108.5	5.07
	48	0.4			116.5	5.44
	60	0.5			123.5	5.77

AppendixA. Additional notations

The following notations are useful for simplifying the linear algebraic equations appear in this paper:

$$a_1 = \lambda_1 L = \frac{1}{\kappa}\hat{P}\sqrt{12\left(1+\frac{1}{\eta}\right)} \tag{A.1}$$

$$a_2 = \lambda_0 L = a_1/b_1 \tag{A.2}$$

$$a_3 = \lambda_2 L = a_1/b_2 \tag{A.3}$$

$$a_4 = \lambda_1 l_A = a_1 q \tag{A.4}$$

$$a_5 = \lambda_0 l_B = a_1 (1-q-r)/b_1 \tag{A.5}$$

$$a_6 = \lambda_2 l_C = a_1 r/b_2 \tag{A.6}$$

where

$$b_1 = \frac{\lambda_1}{\lambda_0} = 2\sqrt{\frac{3I_0}{\Sigma}} \tag{A.7}$$

$$b_2 = \frac{\lambda_1}{\lambda_2} = \sqrt{\frac{1}{\Sigma\eta^3}} \tag{A.8}$$

The eight unknowns, A_1, B_1, A_0, B_0, A_2, B_2, $\hat{R}_A$ and $\hat{M}_A$ in equations (4) to (6) can be computed through simple MATLAB code, upon simplifying the linear algebraic equations with above additional notations.

AppendixB. Energy release rate and mode mixity

AppendixB.1. Left-hand crack tip

The geometric quantities A_e and I_e are defined as [18]:

$$A_e = \frac{1}{\eta} + \Sigma$$

$$I_e = \Sigma\left[\left(\Delta - \frac{1}{\eta}\right)^2 - \left(\Delta - \frac{1}{\eta}\right) + \frac{1}{3}\right] + \frac{\Delta}{\eta}\left(\Delta - \frac{1}{\eta}\right) + \frac{1}{3\eta^3}$$

Lai et al [1] suggests the *global* mode mixity or phase angle could be expressed as:

$$\psi = \tan^{-1}\left(K_{II}/K_I\right) \tag{B.1}$$

where K_{II} and K_I are respectively defined as mode II and mode I stress intensity factor. In complex plane, the phase angle is given as [18]

$$\psi = \tan^{-1}\left[\frac{\Lambda\sin\omega - \cos(\omega+\gamma)}{\Lambda\cos\omega + \sin(\omega+\gamma)}\right] \tag{B.2}$$

in which loading combination Λ is given as

$$\Lambda = \sqrt{\frac{I}{A}}\left[\frac{(C_1 - 1)/(1 + 1/\eta) - C_2\hat{M}_0}{\hat{M}_1 - C_3\hat{M}_0}\right] \tag{B.3}$$

for a left-hand crack tip. To give a standard interpretation on usual non-oscillatory behavior of stress intensity factors expressed by equation (B.1), the bimaterial constant $\varepsilon = 0$ may be considered in equation (B.2). Solution of angular function ω can be obtained from, and γ, I, A, C_1, C_2 and C_3 are geometric factors defined in paper presented by Suo and Hutchinson [18]. It is worthwhile to note that

their solution assumes that the shear force to have negligible influence on stress intensity factors of the bimaterial interface.

AppendixB.2. Right-hand crack tip

Let η^t, Σ^t, A_{e}^t and I_{e}^t be the quantities upon applying 180° transformational rotation for η, Σ, A_{e} and I_{e} respectively. Subsequently, the nondimensional energy release rate for the right-hand crack tip can be written as:

$$\begin{aligned}\hat{G} &= G/\frac{P^2}{(E_1^*+E_2^*)(h_1+h_2)} \\ &= \frac{1}{2}\Bigg\{\left(1+\frac{1}{\Sigma^t}\right)\left[\left(1+\frac{1}{\eta^t}\right)+12\hat{M}_2^2\left(1+\frac{1}{\eta^t}\right)^3\right] \\ &\qquad -(1+\Sigma^t)\left[\frac{(1+1/\eta^t)}{A_{\mathrm{e}}^t}+\hat{M}_0^2\frac{(1+1/\eta^t)^3}{I_{\mathrm{e}}^t}\right]\Bigg\} \end{aligned} \tag{B.4}$$

To determine the mode mixity for the right-hand crack tip, the problem is to be flipped about y-axis so that it is transformed to a left-hand crack tip problem that can be defined in original problem proposed by Suo and Hutchinson [18], which the loading combination is now given as

$$\Lambda = \sqrt{\frac{I}{A}}\left[\frac{C_1/(1+1/\eta)-C_2\hat{M}_0}{-C_3\hat{M}_0}\right] \tag{B.5}$$

where $\hat{M}_2$ and $\hat{M}_0$ are the nondimensional bending moments evaluated at the right-hand crack tip, which are now given by

$$\hat{M}_2 = \frac{M_2(0)}{P(h_1+h_2)} \qquad \text{and} \qquad \hat{M}_0 = \frac{M_0(l_B)}{P(h_1+h_2)}$$